North Pole; (ii) 1.4×10^{16} kg uniformly distributed from one hemisphere to the other; or (iii) 1.1×10^{16} kg from the oceans to land at high latitudes. We suggest that any reasonable model should therefore have a total seasonal transported mass within 40% of 1.0×10^{16} kg. Secondly, models should predict that the load peaks near the poles in their respective late-winter seasons. Thirdly, models should predict that the load's trajectory follows an approximate great circle over the continents (Fig. 3).

From remote sensing, it is known that the mass of snow in the Northern Hemisphere peaks during February to March at 0.3×10^{16} kg (5, 16). Recent analysis in atmospheric research (6) confirms earlier interpretations (7) on the existence of interhemispheric oscillations in atmospheric mass at the level of 0.4×10^{16} kg, which appears to be driven in part by anomalous cooling over snow-covered areas, particularly over Siberia and Canada (17). Our results therefore suggest that the observed pattern of deformation is dominated by winter groundwater storage enhanced by atmospheric pressure. Assuming an upper bound on the net redistributed mass at 1.4×10^{16} kg, we infer the non-snow component of winter groundwater to be $<0.7 \times 10^{16}$ kg.

The load's trajectory over the continents (in approximately the y-z plane) is consistent with the land's ability to sustain loads (unlike the ocean's tendency to rapidly approach equilibrium). An interesting feature of the load moment time series is the asymmetric pattern of z oscillations (Fig. 1) and the rapid southward equatorial crossing of mass (Fig. 3) in May. This is consistent with rapid water runoff, which is known to peak during late spring in the Northern Hemisphere (18). A small y component of load moment also appears during the transition seasons traversing regions of known intense hydrological loading (9) in southeast Asia and South America (Fig. 2). An anomaly in the $\pm y$ direction is apparent during 1996/1997, immediately preceding the 1997/1998 El Niño event. Possible mechanisms that might enhance the y component include an equatorial oscillation in (nonsteric) sea level across the Pacific (driven by wind stress) and anomalous monsoon precipitation over land.

To conclude, we detected a global-scale mode of Earth deformation that we have identified as the response of an elastic Earth to redistribution of surface load, specifically the degree-one spherical harmonic mode that theoretically corresponds to change in the load moment. This mode compresses one hemisphere and expands the opposite hemisphere in such a manner that it does not change Earth's overall shape, but nevertheless stretches its surface and so affects site coordinates. In Earth's center-of-figure frame, the poles appear to be displaced downward by 3.0 mm during their respective win-

ters, and the equator appears to move toward the winter pole by 1.5 mm. Our inversion procedure produces a load moment time series with an annual signal in Earth's polar direction with amplitude 6.6×10^{22} kg m. Stacking reveals that the load moment follows the approximate trajectory of a great circle traversing the continents, peaking at 6.9×10^{22} kg m near the North Pole in winter. These results are consistent with seasonal loading of land surfaces by fluids, corresponding to an annual mass exchange of $1.0 \pm 0.2 \times 10^{16}$ kg between the hemispheres.

References and Notes

1. W. E. Farrell, *Rev. Geophys. Space Phys.* **10**, 761 (1972).
2. E. W. Grafarend, J. Engels, P. Varga, *J. Geodesy* **72**, 11 (1997).
3. T. van Dam, J. M. Wahr, *Phys. Chem. Earth* **23**, 1077 (1998).
4. A. S. Trupin, M. F. Meier, J. M. Wahr, *Geophys. J. Int.* **108**, 1 (1992).
5. B. F. Chao, W. P. O'Connor, A. T. C. Chang, D. K. Hall, J. L. Foster, *J. Geophys. Res.* **92**, 9415 (1987).
6. Z. Guan, T. Yamagata, *Geophys. Res. Lett.* **28**, 263 (2001).
7. K. Trenberth, *J. Geophys. Res.* **86**, 5238 (1981).
8. T. van Dam, G. Blewitt, M. B. Heflin, *J. Geophys. Res.* **99**, 23939 (1994).
9. T. van Dam *et al.*, *Geophys. Res. Lett.* **28**, 651 (2001).
10. M. Greff-Lefftz, H. Legros, *Geophys. J. Int.* **131**, 699 (1997).
11. For deformations up to degree n, a network can be considered "well distributed" if neighboring stations everywhere are spaced much less than 180°/n, which for $n = 1$ implies multiple stations in arbitrary hemispheres.
12. J. L. Chen, C. R. Wilson, R. J. Eanes, R. S. Nerem, *J. Geophys. Res.* **104**, 2683 (1999).
13. Information on relevant GPS station data is provided at www.sciencemag.org/cgi/content/full/294/5550/2342/DC1.
14. P. Davies, G. Blewitt, *J. Geophys. Res.* **105**, 11083 (2000).
15. G. Blewitt, D. Lavallée, *J. Geophys. Res.*, in press.
16. A. T. C. Chang, J. L. Foster, D. K. Hall, *Remote Sens. Lett. Int. J. Remote Sens.* **11**, 167 (1990).
17. J. Cohen, K. Saito, D. Entekhabi, *Geophys. Res. Lett.* **28**, 299 (2001).
18. B. M. Fekete, C. J. Vörösmarty, W. Grabs, *WMO-Global Runoff Data Centre Report 22* (Koblenz, Germany, 1999).
19. We thank J. Wahr and V. Dehant for comments, and IGS for providing data. Supported by U.S. Department of Energy grant DE-FC08-98NV12081, NASA grant SENH99-0325-0015, U.K. Natural Environment Research Council grant GR3/11976, and a University of Nevada Reno international activities grant. We thank NSF for supporting continuation of this research.

A High-Resolution Absolute-Dated Late Pleistocene Monsoon Record from Hulu Cave, China

Y. J. Wang,[1,3] H. Cheng,[2] R. L. Edwards,[2]* Z. S. An,[3] J. Y. Wu,[4] C.-C. Shen,[5] J. A. Dorale[6]

Oxygen isotope records of five stalagmites from Hulu Cave near Nanjing bear a remarkable resemblance to oxygen isotope records from Greenland ice cores, suggesting that East Asian Monsoon intensity changed in concert with Greenland temperature between 11,000 and 75,000 years before the present (yr. B.P.). Between 11,000 and 30,000 yr. B.P., the timing of changes in the monsoon, as established with ^{230}Th dates, generally agrees with the timing of temperature changes from the Greenland Ice Sheet Project Two (GISP2) core, which supports GISP2's chronology in this interval. Our record links North Atlantic climate with the meridional transport of heat and moisture from the warmest part of the ocean where the summer East Asian Monsoon originates.

The Asian and Australian Monsoons are important because they transport heat and moisture from the warmest part of the tropical ocean (the West Pacific Warm Pool) across the equator and to higher latitudes. The East Asian Monsoon, a sub-system of the Asian Monsoon, affects an area east of the Bay of Bengal and the Tibetan Plateau (1). Spring heating of Asia initiates the summer monsoon, which transports northward moisture and heat from north of Australia across the Warm Pool, as far as northern China. The winter monsoon is characterized by cold, dry

Siberian air flowing southward across eastern China, ultimately contributing to the Australian summer monsoon (1).

Plausible factors affecting the monsoon are orbitally controlled changes in insolation (2, 3), shifts in sea level causing changes in Warm Pool surface area (4), and circulation changes internal to the climate system (5). Loess records (6, 7) show clear evidence for monsoon changes (1) that are possibly linked to global climate (7) and Heinrich Events (5). However, resolution and dating problems limit the loess work. We reconstruct mon-

Fig. 1. δ^{18}O of Hulu Cave sta-lagmites (purple, green, and red) and Greenland Ice (*22*) (dark blue) and insolation at 33°N av-eraged over the months of June, July, and August (*20, 21*) (black) versus time. [230]Th ages and er-rors are color-coded by stalag-mite. Numbers indicate GISs and correlated events at Hulu Cave. The YD and Heinrich events are depicted with vertical bars (*24*). The brown and blue bars indicate two possible corre-lations to H5. The average num-ber of years per δ^{18}O analysis is 130 for MSD and 140 for MSL. The δ^{18}O scales are reversed for Hulu (increasing down) as com-pared with Greenland (increas-ing up).
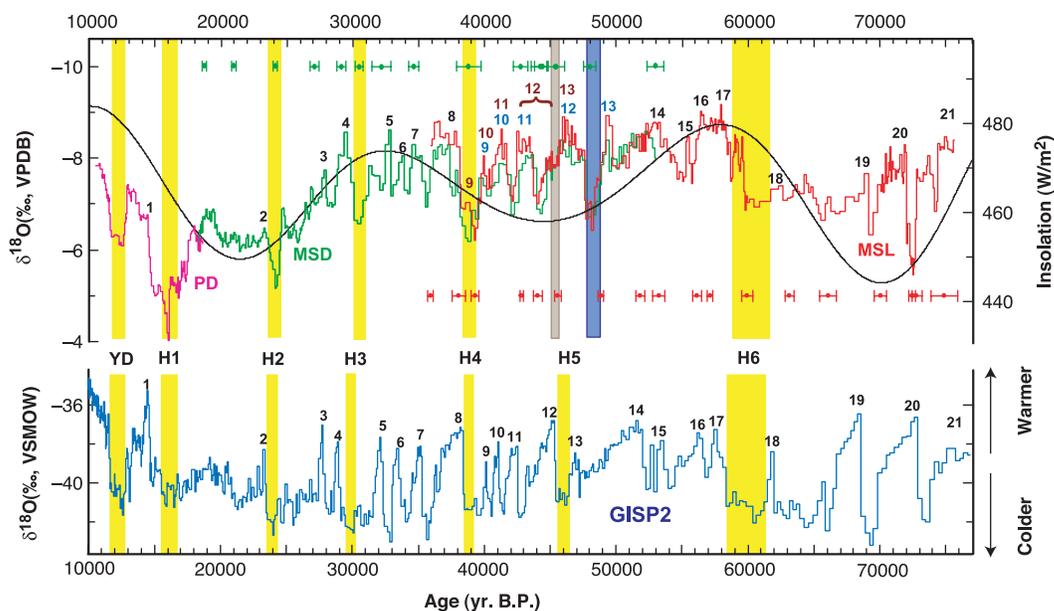
soon history with the oxygen isotopic com-position of speleothem calcite, which has key advantages over many archives of past con-ditions. Well-chosen inorganic calcite can be dated precisely (*8, 9*) with mass spectromet-ric [230]Th methods (*10*). Speleothems may form continuously for tens of thousands of years and can be sampled at high resolution for dating and δ^{18}O analysis.

We collected five stalagmites from 35 m depth in Hulu Cave, 28 km east of Nanjing (32°30′N,119°10′E). We halved samples along growth axes and sub-sampled on cut surfaces for [230]Th dating by thermal ioniza-tion (*10*) and inductively coupled plasma mass spectroscopy (*11, 12*) and δ^{18}O analysis (*13*). Fifty-nine [230]Th dates (Fig. 1) (*14*), all in stratigraphic order, have analytical errors equivalent to about ±150 years at 10,000 years and ±400 years at 60,000 years. The oldest age is 74,875 ± 1,010 yr. B.P. (relative to 1950 A.D.) and the youngest is 10,933 ±160 yr. B.P., with at least one stalagmite active during all intervening times. Sample YT has visible banding throughout, and three [230]Th ages with errors of ±60 to ±90 years. Numbers of bands are equal to differences in age between dated sub-samples, indicating that the banding is annual. We established the time scale for sample H82 with two [230]Th
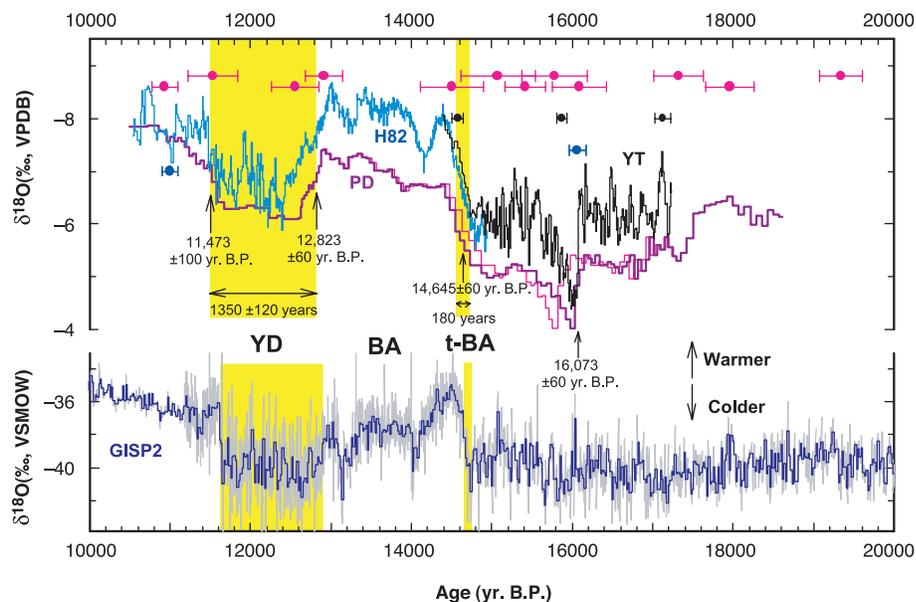

Fig. 2. δ^{18}O of Hulu stalagmites (purple, black, and blue) and Greenland Ice (*22*) (dark blue shows 20-year averages; gray shows 3-year averages) versus time. Yellow bands indicate the timing and duration of the YD and the transition into the BA (t-BA); the BA is the interval between the yellow bands. [230]Th ages and errors are color-coded by stalagmite. The chronology of YT and most of the chronology of H82 are fixed by annual banding. As YT and H82 are more precisely and continuously dated than PD, we adjusted the time scale of PD between 17 and 14 ka to match the major δ^{18}O features. The slight adjustment is well within the errors of the PD time scale. The thin δ^{18}O trace in this interval depicts the PD record based solely on its own [230]Th dates. The average number of years per δ^{18}O analysis is 60 for PD, 9 for YT, and 7 for H82.

[1]College of Geography Science, Nanjing Normal Uni-versity, Nanjing 210097, China. [2]Department of Ge-ology and Geophysics, University of Minnesota, MN 55455, USA. [3]State Key Laboratory of Loess and Quaternary Geology, Institute of Earth Environment, Chinese Academy of Sciences, Xi'an 710054, China. [4]State Key Laboratory for Mineral Deposits Research, Nanjing University, Nanjing 210008, China. [5]Depart-ment of Earth Sciences, National Cheng Kung Univer-sity, Tainan, Taiwan, China. [6]Department of Geological Sciences, University of Missouri, Columbia, MO, USA.

*To whom correspondence should be addressed: E-mail: edwar001@umn.edu

ages (Fig. 2) (*14*), by matching its oxygen isotope record to YT's at 14.6 thousand years ago (ka), and by band counting between 11.0 and 11.8 ka and between 13.0 and 14.6 ka.

A key issue is whether calcite δ^{18}O can be interpreted solely in terms of the δ^{18}O of meteoric precipitation and equilibrium frac-tionation during calcite precipitation. Hendy (*15*) described additional processes (e.g., ki-netic fractionation) that could also affect δ^{18}O. A robust test is the comparison of δ^{18}O

for contemporaneous stalagmites from the same cave (*16*). If the records replicate, the net effect of additional processes on δ^{18}O must have been the same. Consistent offsets are unlikely because each stalagmite-precip-itating drip has a unique combination of flow path, CO_2 partial pressure, residence time, concentration of solutes, and degassing his-tory. Thus, replicated records strongly sug-gest that such additional processes are not important. With modern dating and δ^{18}O

Fig. 3. Difference in age between Hulu and Greenland ice core time scales [GRIP, (*23*); GISP2, (*25*)] versus Hulu age. Each point is based on a correlation between GRIP or GISP2 and Hulu (e.g., the correlations between Hulu and the GIS's depicted in Fig. 1). Positive values are times when the ice core age is less than the Hulu age; negative values are times when the ice core age is more than the Hulu age. Typical ^{230}Th dating errors as a function of time are illustrated by the gray error envelope where the difference in age is 0. Error bars are estimates of the error in the ice core chronologies (*23*, *25*).
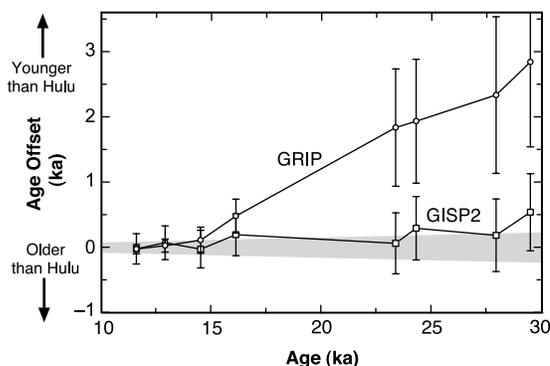
measurement techniques, the replication test can be made with high resolution and little temporal ambiguity.

Stalagmites MSD and MSL (Fig. 1) (*14*) grew contemporaneously between 53 and 36 ka. Considering dating errors and resolution differences, the records are virtually identical over this interval. At least two stalagmites (out of PD, YT, and H82) grew contemporaneously for all times between 17 and 10.5 ka (Figs. 1 and 2) (*14*). Samples YT and H82, both sampled at high resolution, have an overlapping section with δ^{18}O values that replicate. Sample PD was sampled at lower resolution and has δ^{18}O values offset from the others by a small amount (about 0.5‰) compared with the 5‰ amplitude of the record. Nevertheless, the pattern of δ^{18}O variation is similar among overlapping sections of all five stalagmites, suggesting we can treat them as replicated records. We also tested for positive correlation between δ^{13}C and δ^{18}O values, plausibly indicative of kinetic fractionation (*15*). R^2 values are either low or the correlation is negative for each of six data groupings [data for each of five speleothems grouped individually and as one group; see (*14*)], thus showing no evidence for kinetic fractionation.

Given records that replicate and the lack of a clear positive correlation between δ^{13}C and δ^{18}O values, the issue becomes how to interpret the record in terms of the δ^{18}O of precipitation and temperature. Mean annual rainfall and temperature at Hulu Cave are 1015 mm and 15.4°C. The summer monsoon (June to September) contributes 80% of annual precipitation with $\delta^{18}O_{VSMOW}$ of −9‰ to −13‰. The rest comes during the winter monsoon with δ^{18}O about 10‰ higher (−3 to +2‰) (*17*). Because of the large seasonal difference, a mechanism that may explain large changes in past mean annual δ^{18}O of precipitation is a change in the ratio of the amount of summer to winter precipitation. Temperature effects are likely to be small because changes in the temperature-dependent fractionation between calcite and water are small (on the order of −0.25‰/°C) (*18*).

On the basis of modern data (*19*), the effects of summer temperature and rainfall amount on mean δ^{18}O of summer precipitation are also small, with similar relations holding for winter (*19*).

Hulu Cave δ^{18}O values range from −4 to −9‰ between 75 and 10 ka (*14*). The large range suggests that a primary control is variance in the summer/winter precipitation ratio. If so, a change in the ratio by a factor of 3 (from today's value of 4 to 1.3) is required to explain the 5‰ amplitude. This factor is likely an upper limit because temperature and amount effects may also contribute.

The long-term Hulu trend (Fig. 1) appears to follow summer (integrated over June, July, and August) insolation (*20*, *21*) at Hulu Cave (33°N), at least for a good portion of the record, suggesting that high summer insolation increases the continent-ocean temperature difference, enhancing the summer monsoon (*2*, *3*). However, the record is punctuated by numerous millennial-scale events and by shifts in δ^{18}O over centuries or less, much shorter than orbital time scales.

These features resemble the Greenland ice-core δ^{18}O records (*22*, *23*). If analogous features do represent coincident events, Greenland temperature correlates positively with the summer/winter precipitation ratio in eastern China. To the extent that changes in the ratio result from changes in summer precipitation, warmer Greenland temperatures correlate with a more intense summer East Asian Monsoon. Between 10 and 15 ka, an interval for which ice core chronologies are robust, we can test for synchronicity. In this interval, samples PD and H82 (Fig. 2) exhibit features similar to the Younger Dryas (YD) and the Bolling-Allerod (BA). On the basis of independent time scales, these features are synchronous within errors (Fig. 2), demonstrating a link between the East Asian Monsoon and Greenland temperatures.

In detail, there are both similarities and differences in the Hulu and Greenland deglacial sequences (*22*, *23*). The Hulu record has a sharp increase (about 2‰) in δ^{18}O at 16,073 ± 60 yr. B.P., which takes place in

<20 years, at about the time of Heinrich Event 1 (H1) (*24*). A similar feature is not apparent in the ice records. The slopes of the records during the BA differ, which could result, in part, from the decrease in marine δ^{18}O associated with glacial melting, because this would affect the records in opposite senses. The most rapid portion of the transition into the BA appears to be more gradual at Hulu (180 years by band counting centered at 14,645 ± 60 yr. B.P.) as compared with Greenland (about 100 years centered at about 14,680 ± 290 yr. B.P. in GISP2). In contrast, the transition at the beginning of the YD (12,823 ± 60 yr. B.P. at Hulu and 12,880 ± 260 yr. B.P. in GISP2) is of similar short duration (<20 years). The transition ending the YD [11,473 ± 100 yr. B.P. at Hulu, 11,550 ± 70 yr. B.P. in the Greenland Ice Core Project (GRIP) (*23*), and 11,640 ± 250 yr. B.P. in GISP2 (*22*)] is also extremely rapid at both localities (<10 years). The duration of the YD as recorded at Hulu (1350 ± 120 years) is the same within error as its duration in Greenland.

Given the apparent synchronicity between Hulu and Greenland for times when the ice core chronologies are robust, we may correlate older events, for which ice core chronologies are less certain (Fig. 1). This correlation appears straightforward as far back as 38 ka. The highest Hulu δ^{18}O values (at 16,032 ± 60 yr. B.P.) correspond to low Greenland temperatures associated with H1. Low Hulu δ^{18}O values (at 23,310 ±100 yr. B.P.) correspond to Greenland Interstadial (GIS) 2, which is immediately preceded by high δ^{18}O values (24,180 ±100 yr. B.P.) corresponding to low Greenland temperatures associated with H2. Low δ^{18}O excursions correspond to GIS 3 through 8 (Fig. 1). With these correlations, we assign times to Greenland events with Hulu ages. For times between GIS 1 and 8, age offsets between GISP2 and Hulu are less than several hundred years, whereas offsets between GRIP and Hulu increase progressively from 0 at 15 ka to 3000 years at 30 ka (Fig. 3). For this interval, GISP2's time scale, determined by band counting (*25*), appears robust. For times older than ~15 ka, the GRIP time scale was determined by flow modeling, with primary accumulation rates estimated by ice δ^{18}O values (*23*). In Greenland, the 15 to 30 ka interval is characterized by low δ^{18}O and low accumulation rates. Of the many factors that contribute to the construction of each time scale, we cannot uniquely identify those that contribute to discrepancies between time scales. However, use of a somewhat lower accumulation rate for GRIP in this cold interval would largely reconcile the three chronologies between 15 and 30 ka.

For GIS 9 through 13, we present two possible correlations. Those represented by

blue numbers (Fig. 1) appear to follow logically as we correlate peaks back from GIS 8. However, this correlation places the beginning of GIS 12 (the end of H5) at 48 ka. Both GISP2 (*25*) and GRIP (*23*) as well two other high-precision stalagmite records place the end of H5 at ∼45 ka (*26, 27*). The differences among stalagmite records [Hulu, Sorel Cave, Israel (*26*), and Crevice Cave, Missouri (*27*)] highlight important regional differences in past climate at this time. If we take the end of H5 at 45 ka as a tie point, we obtain the correlation depicted by the brown numbers. At present, we cannot distinguish between the two. Beyond GIS 13, the correlation appears straightforward and is consistent with the only other high-resolution speleothem correlation that covers this whole time range (*27*). The oldest part of our record correlates to the end of GIS 21.

The Hulu record identifies a link between the East Asian Monsoon and North Atlantic climate and supports the idea that millennial-scale events first identified in Greenland are hemispheric or wider in extent (*28–32*). The Greenland events have been explained by changing rates of North Atlantic deep water formation, resulting in changing heat transport to the North Atlantic (*28, 33*). The millennial-scale changes that we observe may result similarly from massive and rapid changes in oceanic and atmospheric circulation patterns. The temporal relations between the Hulu and Greenland deglacial sequences are consistent with North Atlantic events that trigger large-scale circulation changes (*28*). Regardless of the trigger, our observations are consistent with the idea that Northern Hemisphere atmospheric circulation patterns are more meridional in character during Greenland interstadials and are more zonal during stadials. Our data support the idea that changes in the East Asian Monsoon are integral to millennial-scale changes in atmospheric/oceanic circulation patterns and are affected by orbitally induced insolation variations; however, our data do not show clear evidence that sea level itself has an observable effect on East Asian Monsoon intensity.

References and Notes
1. Z. S. An, *Quat. Sci. Rev.* **19**, 171 (2000).
2. J. E. Kutzbach, *Science* **214**, 59 (1981).
3. S. C. Clemens, D. W. Murray, W. L. Prell, *Science* **274**, 943 (1996).
4. P. Wang, *Marine Geology* **156**, 5 (1999)
5. S. C. Porter, Z. S. An, *Nature* **375**, 305 (1995).
6. T. S. Liu, Ed., *Loess and Environment* (China Ocean Press, Beijing, 1985), pp. 168–183.
7. G. Kukla *et al.*, *Geology* **16**, 811 (1988).
8. W. X. Li *et al.*, *Nature* **339**, 534 (1989)
9. K. R. Ludwig *et al.*, *Science* **258**, 284 (1992).
10. R. L. Edwards, J. H. Chen, G. J. Wasserburg, *Earth Planet. Sci. Lett.* **81**, 175 (1987).
11. X. Luo, M. Rehkämper, D. Lee, A. N. Halliday, *Inter. J. Mass Spectrom. Ion Proc.* **171**, 105 (1997).
12. C. C. Shen *et al.*, *Chem. Geol.*, in press.
13. δ18O values were determined on a Finnigan MAT 251 (Bremen, Germany) at the Nanjing Institute of Geology and Paleontology, Chinese Academy of Sciences. The GBW4405 carbonate powder standard (a Chinese National Material Standard from the Chinese National Standards Bureau) was used as a reference standard and run every nine samples. The mean and standard deviation of the population of 338 standard runs was −8.56 ± 0.08‰ (relative to VPDB) for δ18O, as compared with the Standards Bureau value of −8.49‰.
14. Supplemental data are available at *Science* Online at www.sciencemag.org/cgi/content/full/294/5550/2345/DC1.
15. C. H. Hendy, *Geochim. Cosmochim. Acta* **35**, 801 (1971).
16. J. A. Dorale, R. L. Edwards, E. Ito, L. A. González, *Science* **282**, 1871 (1998).
17. S. Zheng *et al.*, *Chinese Sci. Bull.* **13**, 801 (1983).
18. I. Friedman, J. R. O'Neil, *U.S. Geol Surv. Prof. Paper* 440-KK (1977), p. 3.
19. B. Li, D. Yuan, J. Qin, Y. Lin, M. Zhang, *Sci. China Ser. D* **43**, 227 (2000).
20. A. Berger, *J. Atmos. Sci.* **35**, 2362 (1978).
21. D. Paillard, L. Labeyrie, P. Yiou, *EOS* **77**, 379 (1996).
22. The Greenland Summit Ice Cores [CD-ROM], 1997. Available from the National Snow and Ice Data Center, University of Colorado at Boulder, and the World Data Center-A for Paleoclimatology, National Geophysical Data Center, Boulder, CO. Also available online at: www.ngdc.noaa.gov/paleo/icecore/greenland/summit/index.html.
23. W. Dansgaard *et al.*, *Nature* **364**, 218 (1993).
24. G. C. Bond *et al.*, *Nature* **365**, 143 (1993).
25. D. A. Meese *et al.*, *J. Geophy. Res.* **102**, 26411 (1997).
26. M. Bar-Matthews, A. Ayalon, A. Kaufman, G. J. Wasserburg, *Earth Planet. Sci. Lett.* **166**, 85 (1999).
27. J. A. Dorale, thesis, University of Minnesota (2000).
28. W. S. Broecker, *Nature* **372**, 421 (1994).
29. M. Kienast *et al.*, *Science* **291**, 2132 (2001).
30. I. Hendy, J. Kennett, *Geology* **27**, 291 (1999).
31. K. A. Hughen, J. R. Southon, S. J. Lehman, J. T. Overpeck, *Science* **290**, 1951 (2000).
32. H. Schulz *et al.*, *Nature* **393**, 54 (1998).
33. D. Roemmich, *J. Phys. Oceanogr.* **10**, 1972 (1981).
34. We thank two anonymous reviewers for constructive criticisms that improved this contribution considerably. Supported by National Natural Science Foundation of China grant 49972055, U.S. NSF grants EAR-9712037 and ESH-9809459, and Chinese Academy of Sciences grants KZCX2-108 and KZCX1-Y-05.

20 July 2001; accepted 7 November 2001

Resolution of the Early Placental Mammal Radiation Using Bayesian Phylogenetics

William J. Murphy,[1]* **Eduardo Eizirik,**[1,2]* **Stephen J. O'Brien,**[1]†
Ole Madsen,[3] **Mark Scally,**[4,5] **Christophe J. Douady,**[4,5]
Emma Teeling,[4,5] **Oliver A. Ryder,**[6] **Michael J. Stanhope,**[5,7]
Wilfried W. de Jong,[3,8] **Mark S. Springer**[4]†

Molecular phylogenetic studies have resolved placental mammals into four major groups, but have not established the full hierarchy of interordinal relationships, including the position of the root. The latter is critical for understanding the early biogeographic history of placentals. We investigated placental phylogeny using Bayesian and maximum-likelihood methods and a 16.4-kilobase molecular data set. Interordinal relationships are almost entirely resolved. The basal split is between Afrotheria and other placentals, at about 103 million years, and may be accounted for by the separation of South America and Africa in the Cretaceous. Crown-group Eutheria may have their most recent common ancestry in the Southern Hemisphere (Gondwana).

Deciphering higher level relationships among mammalian orders is a difficult problem in systematics (*1–6*) and has important ramifications for evolutionary biology, genomics, and biomedical sciences (*7, 8*). Studies based on different, multikilobase molecular data sets (*5, 6*) independently resolved placental mammals into four superordinal groups: Afrotheria, Xenarthra, Laurasiatheria, and Euarchontoglires. However, hierarchical relationships within these groups and at deeper levels in the placental tree remain unclear. A precise resolution of the relationships among the major groups and elucidation of the root of the placental tree are critical for interpreting biogeographic patterns and evolutionary processes involved in the early diversification of placental mammals.

We combined and expanded the large data sets of Madsen *et al.* (*5*) and Murphy *et al.* (*6*) to yield a 16,397–base pair molecular data set that includes 19 nuclear and 3 mitochon-

[1]Laboratory of Genomic Diversity, National Cancer Institute, Frederick, MD 21702, USA. [2]Department of Biology, University of Maryland, College Park, MD 20742, USA. [3]Department of Biochemistry, University of Nijmegen, Netherlands. [4]Department of Biology, University of California, Riverside, California 92521, USA. [5]Queen's University of Belfast, Biology and Biochemistry, Belfast, UK. [6]Center for Reproduction of Endangered Species, Zoological Society of San Diego, San Diego, CA 92112, USA. [7]Bioinformatics, GlaxoSmithKline, Collegeville, PA 19426, USA. [8]Institute for Systematics and Population Biology, Amsterdam, Netherlands.

*These authors contributed equally to this work.
†To whom correspondence should be addressed. E-mail: mark.springer@ucr.edu (M.S.S.) or obrien@ncifcrf.gov (S.J.O.)